THE JOURNAL OF PHYSICAL CHEMISTRY B

ARTICLE

pubs.acs.org/JPCB

# Electrophoresis of a Charge-Regulated Sphere Normal to an Air−Water Interface

Peter Tsai, Hsuan Fang, and Eric Lee*

Department of Chemical Engineering, National Taiwan University, Taipei 10617, Taiwan

**ABSTRACT:** The electrophoresis of a charge-regulated sphere normal to an air−water interface is investigated theoretically. The charge-regulated surface considered here is the generalization of conventional constant surface potential and constant surface charge density situations and models excellently well biocolloids or particles coated with a thin film of polyelectrolytes. The thickness of the double layer surrounding the particle can be arbitrary. A pseudospectral method based on Chebyshev polynomials is employed to solve the governing electrokinetic equations. We found, among other things, that the electric potential on the particle surface is the most dominant factor in the determination of the eventual particle electrophoretic mobility. The larger the number of dissociated functional groups on the particle surface ($N_s$), the higher the absolute surface potential of the particle and hence the larger the magnitude of the mobility. Moreover, the electric potential on the particle surface depends on both the concentration of dissociated hydrogen ions, $[H^+]_0$, and the concentration of electrolytes, $\kappa a$, in the solution. If $[H^+]_0$ and/or $\kappa a$ are small, the bulk condition is advantageous to the dissociation reaction, yielding a higher surface density (higher surface potential) and hence a higher mobility. The air−water interface retards the particle motion in general, especially when the double layer is thick enough to touch the interface. Up to around 60%, reduction of the mobility is observed for some situation. The boundary effect disappears as the double layer gets very thin. This is mainly due to the buildup of the electric potential at the interface right in front of the particle, which in turn generates a repulsive electrostatic force. Comparison with a solid planar wall is carried out to highlight the fundamental nature of the air−water interface, such as the unique phenomenon of the electric potential buildup mentioned above.

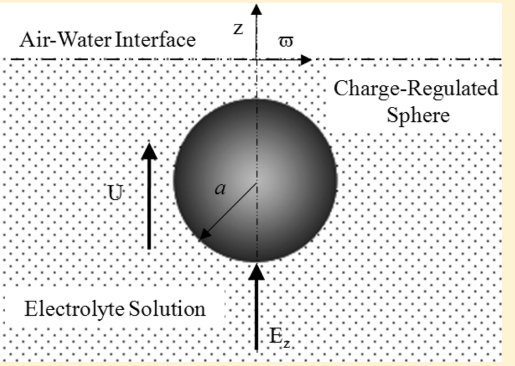


## 1. INTRODUCTION

An air−water interface is encountered very often in many important applications of colloid science. Colloidal crystallization,[1−3] for instance, is a typical example where colloidal particles are trapped at the air−water interface. Aggregations of particles and adsorption of proteins at an air−water interface, on the other hand, find wide applications in formulation and stabilization of products in the biological and food industries.[3] There is much literature dealing with the particle−interface interaction leading to adsorption and trapping or aggregation and clustering of colloidal spheres already at the air−water interface[2] with a view to understanding their structures, growth, and dynamics. The study of colloids near and at the air−water interface is useful also with respect to some biologically oriented questions, revealing some aspects of the crystallization of proteins, which, in a first primitive approach, can be regarded as charged colloids.

A vertical electric field is often applied across the interface to explore the various properties at the interface, and many interesting outcomes have been reported by researchers with different motivations,[4−6] ranging from the fabrication of two-dimensional colloidal crystals to the variation of surface tension with it. These studies are all of experimental nature though. Few theoretical studies have been reported.

As for the electrokinetics involving particle motion near an air−water interface, Huddeson and Smith[7] and Usui and Healy[8] developed a technique based on particle electrophoresis to determine the zeta potential of an air−water interface experimentally. Gao and Li[9] studied the electrophoresis of a particle parallel to a liquid−fluid planar interface, motivated by its potential application in microfluidic operations. On the basis of the thin electric double layer assumption, they obtained analytical solutions of the forces acting on the particle and found that the speed of the particle's electrophoretic motion will increase as the particle−interface distance decreases. Moreover, this enhancement of the electrophoretic mobility becomes more significant with the increase of the viscosity of the second fluid and the decrease of the separation distance. The applied electric fields, however, are all parallel to the free surface in the above electrophoresis analyses.

Recently, the electrophoretic motion of a spherical particle normal to an air−water interface has been investigated theoretically.[10] The surface potential of the particle is assumed constant there. It was found that the presence of the air−water interface reduces the particle mobility in general, especially when the double layer is thick. This boundary effect diminishes as the double layer gets very thin. Moreover, the higher the surface potential, the more significant the reduction of mobility due to the additional

**Received:** January 5, 2011
**Revised:** April 13, 2011
**Published:** May 03, 2011





dx.doi.org/10.1021/jp2000915 | J. Phys. Chem. B 2011, 115, 6484–6494

polarization effect. Local extrema are observed in the mobility profiles with varying double layer thickness as a result. However, the assumption of constant surface potential can be unrealistic in particles. For biocolloids and particles covered by an artificial membrane, for instance, the surface of an entity usually contains dissociable functional groups, the dissociation of which leads to fixed surface charges. In this case, because the degree of dissociation of the functional groups depends on the conditions of the liquid phase, the so-called charge-regulated surface assuming constant surface properties becomes inadequate. As pointed out by Krozel and Saville,[11] constant surface potential and constant surface charge density are idealized conditions that represent two limiting cases, and in practice, the charged condition is between these two limits.

Various investigations on the charge-regulated surface have been reported, both in the fields of electrostatics and electrokinetics.[11−26] Among them, Carnie and Chan[13−16] conducted a series of theoretical investigations about electrostatic interactions between two spherical particles. They observed that the electrostatic interaction or interaction free energy predicted by the charge-regulation model is always intermediate between that predicted by the constant-charged model and the constant-potential model. Menon and Zydney[17] then extended it further to consider a spherical particle in a cylindrical pore. Kuo et al.[18] evaluated the deposition rate of charge-regulated biocolloids on a charged surface. In recent years, Hong and Brown[19,20] studied the electrostatic behavior of the charge-regulated bacterial surface, which plays an important role in bacterial interactions with other surfaces and in bacterial adhesion. As for the electrokinetics involving particle motion, Lee and his co-workers[21−23] considered the electrophoresis of charge-regulated particles. They showed that the number of the functional groups on the particle surface and the pH of the liquid phase have profound impact on the electrophoretic mobility of the particles. The assumptions of constant surface charge density and constant surface potential were served as two limiting cases for the combined electrostatic and hydrodynamic interaction effects on the charge-regulated surfaces. Under essentially the same assumptions, Hsu and his co-workers[24−26] further extended this approach to study several different kinds of boundary effects in electrophoresis. It should be noted that there is a fundamental difference between a solid boundary and a free surface such as the air−water interface. For example, the electrolyte solution in contact with a solid wall is immobile, whereas it is mobile at a free interface. The motion of the electrolyte nearby greatly affects the interfacial electric potential and hence the particle motion. Moreover, perhaps the fundamental difference between the two boundaries in terms of electrostatic interaction can be best illustrated by the image−charge analogue in electrostatics.[27] As a result, the conventional boundary conditions and analyses regarding a solid−liquid interface are not directly applicable to a free surface. Corresponding studies on the electrokinetic motion of charged regulated particles, however, is still missing.

In the present study, we consider the electrophoretic behavior of a charge-regulated sphere normal to an air−water interface. A pseudospectral method based on Chebyshev polynomials is applied here to solve the governing general electrokinetic equations numerically. The method has been successful in solving numerous electrokinetic problems.[10,21−23,28,29] Crucial parameters are analyzed for their impact on the particle motion, such as the dissociation level of the particle surface, the double layer thickness surrounding the particle, and so forth. The separation distance between the particle and the interface is examined in detail, in particular, to highlight the impact of the interface. Moreover, an in-depth comparison is conducted between an air−water interface and a corresponding solid planar wall, focusing on their distinctive impact on the particle motion.

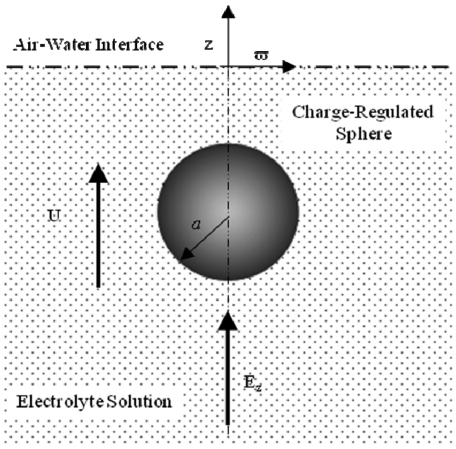


**Figure 1.** Geometric configuration of the system in this study.

## 2. THEORY

As shown in Figure 1, we consider that a charge-regulated spherical particle of radius $a$ moving with a velocity $\mathbf{U}$ is response to an applied electric field $\mathbf{E}$. The particle is suspended in an electrolyte solution that contains a $z_1/z_2$ electrolyte, $z_1/z_2$ being, respectively, the valences of cations and anions. $\alpha$ is defined as $-z_1/z_2$, for example, $\alpha = 1$ for KCl. The electroneutrality in the bulk liquid phase requires that $n_{20} = n_{10}/\alpha$, $n_{10}$ and $n_{20}$ being, respectively, the bulk concentrations of cations and anions. The separation distance between the particle and the interface is denoted as $h$.

The bispherical coordinates $(\xi,\eta,\varphi)$ are used to describe the system. The bispherical coordinates used here are related to the cylindrical coordinates $(r,\theta,z)$[30] as follows

$$z = c\frac{\sinh \eta}{\cosh \eta - \cos \xi} \tag{1}$$

$$\varpi = c\frac{\sin \xi}{\cosh \eta - \cos \xi} \tag{2}$$

where $c$ is the focal length. We define $\eta_0 = -\cosh^{-1}(h/a)$. $\eta = 0$ and $-\eta_0$ represent, respectively, the air−water interface and the surface of the particle.

Major assumptions in our analysis are summarized and discussed as follows. First of all, the Reynolds number of the fluid is assumed to be small enough to justify the use of the Stokes equation, which is essentially always satisfied as the colloidal particle is so small. Moreover, the suspending liquid solution is assumed incompressible as well. The externally applied field $\mathbf{E}$ is weak enough to justify a linear perturbation analysis. In practice, this means that $\mathbf{E}$ is small in comparison with the characteristic electric field across the double layer surrounding the particle, that is, $|\mathbf{E}| \ll \zeta_a\kappa$. The characteristic electric field $\zeta_a\kappa$ is defined as the zeta potential of the particle divided by its double-layer thickness. The particle surface is assumed to be nonconducting. Suppose that the movement of the particle is so slow that the system is at

quasi-steady state and the distribution of ions follows the Boltzmann distribution, which is further simplified under the assumption of low surface potential to yield the famous Debye−Hückel equation.[31] The air phase is regarded as both nonconducting and inviscid due to the fact that the dielectric constant of air is very small in comparison with that of water (1:80) and, therefore, so is the viscosity. Moreover, the air−water interface remains planar as the particle approaches it.[2,10,28] Finally, there is no intrinsic charge at the air−water interface.

The last assumption of chargeless air−water interface deserves closer scrutinization. It should be noted that it had been common wisdom to invoke an ion-free layer of electrolyte solutions near the air−water interface, as proposed by Onsager and Samaras[32] and refined by Levin[33] and Ohshima and Matsubara.[34] Recently, the presence of halogen anions at the air−water interface was inferred from laboratory measurements.[35−37] As summarized by Pavel and Douglas[38] regarding the specific ion effects at the air−water interface in a review paper, "some inorganic ions adsorb to the air−water interface while others do not. The idea that some ions exhibit a propensity for the aqueous surface is only a few years old." In order to clarify this phenomenon, Horinek and Netz1[39] using polarizable force field molecular dynamic simulations to obtain the potential of mean force (PMF) for the halide anions and sodium at a hydrophobic self-assembled monolayer. They observed that the heavier ions do adsorb, whereas the small cations are repelled from the interface. The PMF includes image-charge effects, van der Waals interactions between the ion, water, and substrate, and ion hydration. Surprisingly, they found that the total force is repulsive, concluding that the adsorption of large ions at the air−water interface is mostly caused by surface modified ion hydration. Finally, Levin[40] provided a theoretical explanation for this observed ion adsorption propensity. He concluded that alkali-metal cations and fluoride anions are strongly hydrated and are repelled from the air−water interface. On the other hand, heavier halogens such as $Br^-$ and $I^-$, and the monovalent oxy-anions such as $NO_3^-$, $IO_3^-$, and $ClO_4^-$, are unhydrated and, as a result of their polarizability, are significantly adsorbed to the surface. Following the above review of recent observations, the scope of the current study assuming a chargeless interface thus is confined to systems where no ions are adsorbed at the air−water interface. Note that if there is some specific ion adsorption at the air−water interface in the current electrophoresis system, the particle motion may either be enhanced or deterred depending on the polarity of these charges. A negatively charged interface, for instance, tends to enhance the motion of a positively charged particle in comparison with a chargeless interface, whereas it retards the motion of a negatively charged one.

The standard general electrokinetic equations are used here to predict the electrophoretic behavior of the particle. These include the Poisson equation, the modified Stokes equation with an extra term accounting for the electric body force, the modified Nernst−Planck equation taking into account the possible convection contribution, the incompressibility constraint, and the conservation equation of ion flux at quasi-steady state[10]

$$\nabla^2\phi = -\frac{\rho}{\varepsilon} = -\sum_{j=1}^{2}\frac{z_j e n_j}{\varepsilon} \tag{3}$$

$$\mu\nabla^2\mathbf{v} - \nabla p - \rho\nabla\phi = 0 \tag{4}$$

$$\nabla\cdot\mathbf{v} = 0 \tag{5}$$

$$\nabla\cdot\mathbf{f_j} = 0 \tag{6a}$$

$$\mathbf{f_j} = -D_j\left(\nabla n_j + \frac{n_j e z_j}{k_B T}\nabla\phi\right) + n_j\mathbf{v} \tag{6b}$$

where $\phi$, $\mathbf{v}$, and $\mathbf{f_j}$ are, respectively, the electrical potential, the liquid velocity, and the ion flux. $\rho$ and $\varepsilon$ are, respectively, the space charge density and the permittivity of the liquid phase. $k_B$ and $T$ are, respectively, the Boltzmann constant and the absolute temperature. $e$ is the elementary charge, and $n_j$ and $z_j$ are, respectively, the number concentration and the valence of ionic species $j$, $j = 1$ being cations and $j = 2$ being anions. $D_j$ is the diffusion coefficient for ion $j$. $p$ and $\mu$ are, respectively, the pressure and the viscosity of the electrolyte solution.

We assume that the distribution of ions follows the Boltzmann distribution, where the Nernst−Planck equation is satisfied automatically. As a result, the electrical potential $\phi$ can be described by the Poisson−Boltzmann equation as below

$$\nabla^2\phi = -\frac{\rho}{\varepsilon} = -\sum_{j=1}^{2}\frac{z_j e n_{j0}\exp(-z_j e\phi/k_B T)}{\varepsilon} \tag{7}$$

In these expressions

$$\nabla^2 = \frac{x^2}{c^2}\left[\frac{\partial^2}{\partial\eta^2} + \frac{\partial^2}{\partial\xi^2} - \frac{\sinh\eta}{x}\frac{\partial}{\partial\eta} + \frac{\cos\xi\cosh\eta - 1}{x\sin\xi}\frac{\partial}{\partial\xi}\right] \tag{8}$$

where $x = \cosh\eta - \cos\xi$. If the surface potential is low, eq 7 can be approximated by

$$\nabla^2\phi = \kappa^2\phi \tag{9}$$

where $\kappa = [\Sigma_{j=1}^{2} n_{j0}(ez_j)^2/\varepsilon k_B T]^{1/2}$ is the Debye−Hückel parameter. Note that eq 9 is the well-known Debye−Hückel equation, and this linear approximation is reasonably accurate for $z_1 e\phi/k_B T < 2$.[31]

Taking the curl of eq 4 and introducing a stream function $\psi$ to elimlinate eq 5, we have

$$E^4\psi = \frac{x}{\mu c}\left(\frac{\partial\rho}{\partial\xi}\frac{\partial\phi}{\partial\eta} - \frac{\partial\rho}{\partial\eta}\frac{\partial\phi}{\partial\xi}\right)\sin\xi \tag{10}$$

where $E^4 = E^2E^2$, $x = \cosh\eta - \cos\xi$, and

$$E^2 = \frac{x^2}{c^2}\left[\frac{\partial^2}{\partial\eta^2} + \frac{\partial^2}{\partial\xi^2} + \frac{\sinh\eta}{x}\frac{\partial}{\partial\eta} + \frac{1 - \cos\xi\cosh\eta}{x\sin\xi}\frac{\partial}{\partial\xi}\right] \tag{11}$$

The velocity field is defined by the stream function $\psi$ as

$$v_\xi = -\frac{(\cosh\eta - \cos\xi)^2\partial\psi}{c^2\sin\xi\ \partial\eta} \qquad v_\eta = \frac{(\cosh\eta - \cos\xi)^2}{c^2\sin\xi}\frac{\partial\psi}{\partial\xi} \tag{12}$$

Following Henry's classical analysis of electrophoresis,[41,42] the ion cloud surrounding the particle and the flow field are only slightly distorted by a weak electric field applied to it. The electric potential $\phi$ can be expressed as

$$\phi = \phi_e + \delta\phi \tag{13}$$

with $\delta\phi \ll \phi_e$, where $\phi_e$ is the equilibrium electrical potential and $\delta\phi$ the perturbed electrical potential arising from the applied electric field. Note the symbol e denotes the equilibrium state, and $\delta$ represents the perturbed state. We then have

$$\nabla^2\phi_e = \kappa^2\phi_e \tag{14}$$

$$\nabla^2\delta\phi = 0 \tag{15}$$

$$E^4\psi = \frac{x}{\mu c}\times\left[\frac{\partial\rho_e}{\partial\xi}\frac{\partial\delta\phi}{\partial\eta} - \frac{\partial\rho_e}{\partial\eta}\frac{\partial\delta\phi}{\partial\xi}\right] \tag{16}$$

Consider the case where the surface of a particle contains a functional group AH, which is capable of undergoing the dissociation reaction

$$AH \leftrightarrow A^- + H^+ \tag{17}$$

Let $K_a$ be the dissociation constant of this reaction. Then

$$K_a = \frac{[A^-][H^+]_s}{[AH]} \tag{18}$$

where $[\bullet]$ denotes concentration and $[H^+]_s$ is the value of $[H^+]$ at the particle surface. Suppose that the spatial distribution of $[H^+]$ follows the Boltzmann distribution, that is

$$[H^+]_s = [H^+]_0 \exp\left(-\frac{e\phi_e}{k_BT}\right) \tag{19}$$

where $[H^+]_0$ is the bulk value of $[H^+]$. If we let $N_s$ be the concentration of the functional groups on the particle surface, then

$$N_s = [AH] + [A^-] \tag{20}$$

Equations 18−20 lead to

$$[A^-]_s = \frac{N_s}{1 + \frac{[H^+]_0}{K_a}\exp\left(-\frac{e\phi_e}{k_BT}\right)} \tag{21}$$

The charge density on the surface of the representative particle, $\sigma$, is given by

$$\sigma = -e[A^-] \tag{22}$$

Substituting eq 22 into eq 21 yields

$$\sigma = \frac{-eN_s}{1 + \frac{[H^+]_0}{K_a}\exp\left(-\frac{e\phi_e}{k_BT}\right)} \tag{23}$$

If the relative permittivity of the representative particle is much smaller than that of the liquid phase, then

$$\sigma = -\varepsilon\nabla\phi\cdot\mathbf{n} \tag{24}$$

In bispherical coordinates, this expression becomes

$$\sigma = \varepsilon\frac{x}{c}\frac{\partial\phi_e}{\partial\eta} \tag{25}$$

Combining eqs 23 and 25, we obtain

$$\frac{\partial\phi_e}{\partial\eta} = \frac{1}{\varepsilon}\frac{c}{x}\frac{eN_s}{1 + \frac{[H^+]_0}{K_a}\exp\left(-\frac{e\phi_e}{k_BT}\right)} \qquad \eta = -\eta_0 \tag{26}$$

For convenience, scaled quantities are used in the discussion hereafter. Equation 26 can be further reduced to

$$\frac{\partial\phi_e^*}{\partial\eta} = \frac{c^*}{x}\frac{A}{1 + B\exp(-\phi_e^*)} \qquad \eta = -\eta_0 \tag{27}$$

where $c^* = c/a$, $A = ae^2N_s/\varepsilon k_BT$, and $B = [H^+]_0/K_a$. This expression describes the boundary condition at the particle surface. If the potential $\phi_e$ is low, eq 23 can be further simplified by

$$\begin{aligned}\sigma &= \sigma|_{\phi_e=0} + \left.\frac{d\sigma}{d\phi_e}\right|_{\phi_e=0}(\phi_e - 0)\\ &= \frac{-eN_s}{\{1 + [H^+]_0/K_a\}} - \frac{(e^2N_s/k_BT)\{[H^+]_0/K_a\}}{\{1 + [H^+]_0/K_a\}^2}\phi_e\end{aligned} \tag{28}$$

Combining eqs 25 and 28 gives

$$\frac{c^*}{x}\frac{1+B}{A}\frac{\partial\phi_e^*}{\partial\eta} + \frac{B}{1+B}\phi_e^* = -1 \qquad \eta = -\eta_0 \tag{29}$$

Note that eq 29 is a simple linear combination of the constant potential and constant charge situations. For example, it reduces to the constant charge case with $\partial\phi_e^*/\partial\eta = -xA/c^*$ if $B$ is set to 0 and to the constant potential case with $\phi_e^* = -(1 + B)/B$ if $A$ is very large. It should be noted that although there is no such simple mathematical expression in terms of a linear combination as the surface potential gets high, the charge regulation model employed here remains as the general expression for the actual physical situation on the colloid surface.

Other boundary conditions associated with eqs 14 and 15 are

$$\frac{\partial\phi_e}{\partial\eta} = 0 \qquad \eta = 0 \tag{30}$$

$$\frac{\partial\delta\phi}{\partial\eta} = 0 \qquad \eta = -\eta_0 \tag{31}$$

$$\frac{\partial\delta\phi}{\partial\eta} = -E \qquad \eta = 0 \tag{32}$$

$$\frac{\partial\phi_e}{\partial\xi} = \frac{\partial\delta\phi}{\partial\xi} = 0 \qquad \xi = 0, \pi \tag{33}$$

where $E$ is the magnitude of electric field at the "liquid-phase" side of the interface. Equation 30 indicates that the air−water interface is nonconducting and that there is no intrinsic charge at the interface. Hence, the electric flux through the air−water interface is 0.[2,10,28] Equation 32 results from the fact that the dielectric constant of air is much smaller than that of water, and the interface is assumed to be chargless. Equation 33 implies that the $\phi_e$ and $\delta\phi$ are symmetric about the z-direction.

The boundary conditions associated with eq 16 are assumed to be

$$\psi = -\frac{1}{2}\left(\frac{c\sin\xi}{x}\right)^2 U \qquad \eta = -\eta_0 \tag{34}$$

$$\frac{\partial\psi}{\partial\eta} = \frac{c^2}{x^3}\sin^2\xi\sinh\eta U \qquad \eta = -\eta_0 \tag{35}$$


dx.doi.org/10.1021/jp2000915 |J. Phys. Chem. B 2011, 115, 6484–6494

$$\frac{\partial \psi}{\partial \xi} = 0 \qquad \eta = 0 \tag{36}$$

$$\varepsilon \frac{\partial \delta\phi}{\partial \eta}\frac{\partial \phi_e}{\partial \xi} - \mu \frac{x}{c \sin \xi}\frac{\partial^2 \psi}{\partial \eta^2} = 0 \qquad \eta = 0 \tag{37}$$

$$\frac{\partial \psi}{\partial \xi} = \psi = 0 \qquad \xi = 0, \pi \tag{38}$$

where $U$ is the terminal velocity of the particle. Equations 34 and 35 represents that the particle is moving with velocity $U$. Equation 36 indicates that the normal velocity vanishes there as the interface is impenetrable. Equation 37 denotes that a free surface is incapable of sustaining a shear stress.[10] Equation 38 implies the $\psi$ is symmetric around the $z$-direction, where $\psi = 0$ is an arbitrary reference value for the stream function.

Dimensionless variables are then introduced as follows: $r^* = r/a$, $n_j^* = n_j/n_{10}$, $E^* = E/[(k_BT/e)/a]$, $U^* = U/U_E$, $\phi^* = \phi/(k_BT/e)$, and $\psi^* = \psi/U_E a^2$, where the superscript * denotes dimensionless quantities. Note that $U_E$ is defined as $\varepsilon(k_BT/e)^2/\mu a$, which stands for the particle velocity if an electric field $(k_BT/e)/a$ is applied, according to the Smoluchowski's prediction. On the basis of these expressions, the governing equations can be further simplified as

$$\nabla^{*2}\phi_e^* = (\kappa a)^2 \phi_e^* \tag{39}$$

$$\nabla^{*2}\delta\phi^* = 0 \tag{40}$$

$$E^{*4}\psi^* = (\kappa a)^2 \frac{x \sin \xi}{c^*} \times \left[\frac{\partial \delta\phi^*}{\partial \xi}\frac{\partial \phi_e^*}{\partial \eta} - \frac{\partial \delta\phi^*}{\partial \eta}\frac{\partial \phi_e^*}{\partial \xi}\right] \tag{41}$$

The boundary conditions associated with eqs 39−41 are

$$\frac{\partial \phi_e^*}{\partial \eta} = 0 \qquad \eta = 0 \tag{42}$$

$$\frac{\partial \delta\phi^*}{\partial \eta} = 0 \qquad \eta = -\eta_0 \tag{43}$$

$$\frac{\partial \delta\phi^*}{\partial \eta} = -E^* \qquad \eta = 0 \tag{44}$$

$$\psi^* = -\frac{1}{2}\omega^{*2}U^* \qquad \eta = -\eta_0 \tag{45}$$

$$\frac{\partial \psi^*}{\partial \eta} = \frac{c^{*2}}{x^3}\sin \xi \sinh \eta U^* \qquad \eta = -\eta_0 \tag{46}$$

$$\frac{\partial \psi^*}{\partial \xi} = 0 \qquad \eta = 0 \tag{47}$$

$$\frac{\partial \delta\phi^*}{\partial \eta}\frac{\partial \phi_e^*}{\partial \xi} - \frac{1}{\omega^*}\frac{\partial^2 \psi^*}{\partial \eta^2} = 0 \qquad \eta = 0 \tag{48}$$

$$\frac{\partial \phi_e^*}{\partial \xi} = \frac{\partial \delta\phi^*}{\partial \xi} = \frac{\partial \psi^*}{\partial \xi} = \psi^* = 0 \qquad \xi = 0, \pi \tag{49}$$

where $\omega^* = c^* \sin \xi/x$.

According to O'Brien and White,[43] the present problem can be further divided into two subproblems. In the first problem, the particle moves in the absence of the applied electric field, **E**. and in the second problem, an electric field **E** is applied on a stationary particle. In the first problem, the total force acting on a particle in the vertical direction, $F_1$, is proportional to its electrophoretic velocity, **U**, while in the second problem the total force, $F_2$, is proportional to the applied electric field, **E**. Therefore, we have $F_1 = c_1U^*$ and $F_2 = c_2E^*$, where $c_1$ is independent of $U^*$ and $c_2$ is independent of $E^*$. The dimensionless electrophoretic mobility can be defined as $\mu_m^* = U^*/E^*$. The total force on the particle vanishes at the quasi-steady state, that is, $F_1 + F_2 = 0$, and $\mu_m^*$ can thus be expressed as $\mu_m^* = U^*/E^* = -c_2/c_1$. The total force acting on a particle $F_i$ is comprised of the electric force $F_{ie}$ and the hydrodynamic force $F_{id}$, where the subscript $i$ represents subproblems 1 and 2. Once $F_{ie}$ and $F_{id}$ are evaluated, $c_i$ and $\mu_m^*$ can be obtained accordingly. The details of the numerical procedure can be found elsewhere.[23] Corresponding formulas evaluating force terms in the dimensionless form are given as follows

$$F_{ie}^* = 2\pi \int_0^\pi -\frac{\sin \xi \partial \phi^*}{x \quad \partial \eta} \times \left((1 - \cosh \eta \cos \xi)\frac{\partial \phi^*}{\partial \eta} - \sinh \eta \sin \xi \frac{\partial \phi^*}{\partial \xi}\right) d\xi \tag{50}$$

$$F_{id}^* = \pi \int_0^\pi -\omega^{*3}\frac{\partial}{\partial \eta}\frac{E^{*2}\psi^*}{\omega^{*2}}\, d\xi + (\kappa a)^2 \pi \int_0^\pi \frac{c^{*2}}{x^2}\sin^2 \xi \phi^* \frac{\partial \phi^*}{\partial \xi}\, d\xi \tag{51}$$

## 3. RESULTS AND DISCUSSION

The convergence of the numerical scheme is assured by a standard mesh refinement test. A mesh with 30 × 60 nodal points in the $(\xi,\eta)$ domain is found to be sufficiently accurate in that the results do not vary any more with an even finer mesh, which is used to carried out the calculations in this study. Figure 2A depicts the absolute scaled mobility $|\mu_m^*|$ (defined as $|\mu_m^*| = |\mu_m|/(\varepsilon k_BT/\mu e)$) when the particle is far away from the interface ($h^* = h/a = 80$) as a function of $\kappa a$ (defined as $\kappa a = a/[\sum_{j=1}^{2} n_{j0}(ez_j)^2/\varepsilon k_BT]^{-1/2}$, where $\kappa$ is the Debye−Hückel parameter.). Note that the reciprocal of $\kappa a$ represents the double-layer thickness. The larger the $\kappa a$ value, the thinner the double layer, and vice versa. Corresponding results of the absolute scaled surface potential of the particle $|\phi_e^*|$ is illustrated in Figure 2B as well. Note that at such a remote distance from the air−water interface, the presence of the interface is hardly "felt" by the particle,[2] and the system is very similar to a single particle suspended in an infinite medium. As shown in Figure 2, the results presented in this study approach those of the theoretical predictions made by Lee et al.[21] earlier for a very dilute suspension of charged-regulated spherical particles. This serves as an additional verification of this study for limiting cases. Moreover, we compare our theoretical predictions with a related study reported by Heard and Seaman,[44] where the electrophoretic mobility of a dilute suspension of Human Red Cell was investigated. Our results agree very well with their experimental data when the air−water interface is far away from the particle. The agreement with

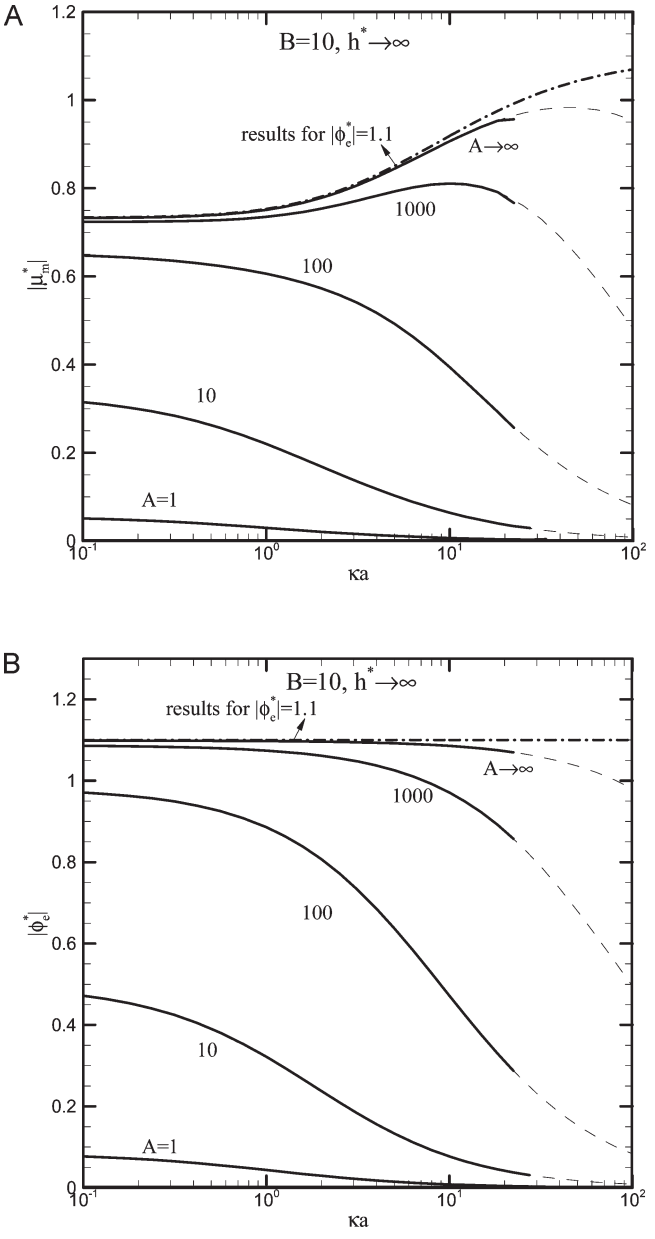


**Figure 2.** (A) Scaled mobility as a function of $\kappa a$ at different $A$ with $B$ = 10 and $h^*$ = 80. Dashed lines: results based on a cell model approach with a very dilute volume fraction. Dashed−dotted line: results based on the constant potential boundary condition. (B) Scaled surface potential as a function of $\kappa a$ at different $A$ with $B$ = 10 and $h^*$ = 80. Dashed lines: results based on a cell model approach with a very dilute volume fraction. Dashed−dotted line: results based on the constant potential boundary condition.

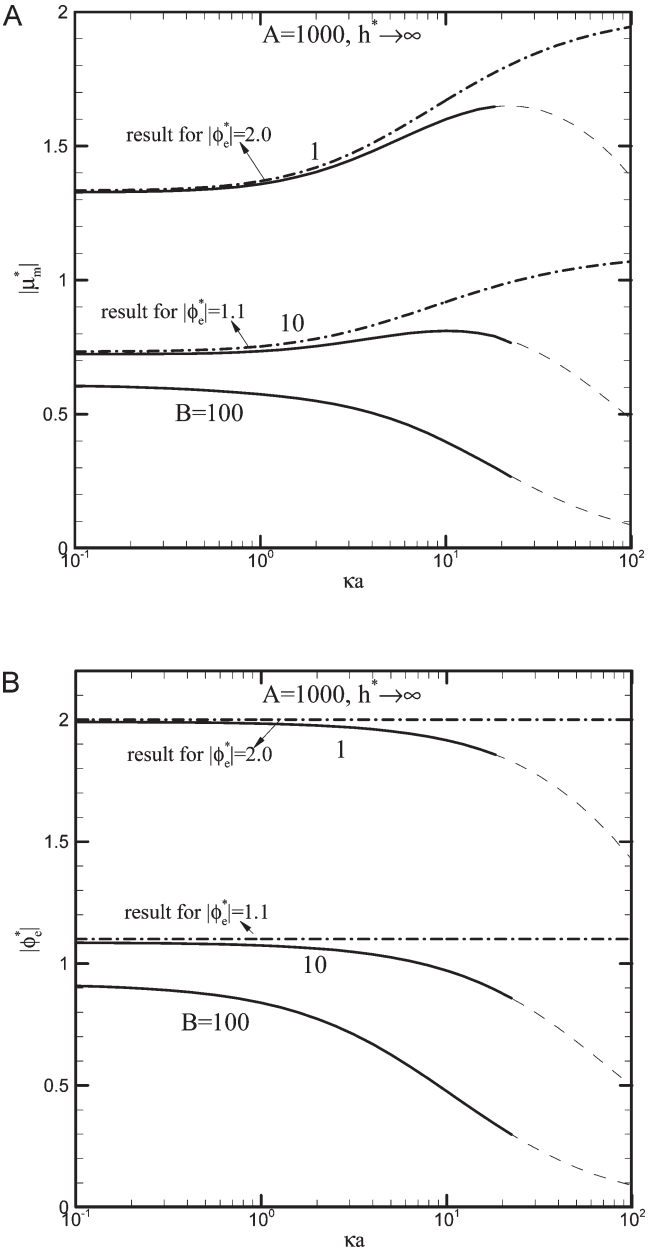


**Figure 3.** (A) Scaled mobility as a function of $\kappa a$ at different $B$ with $A$ = 1000 and $h^*$ = 80. Dashed lines: results based on a cell model approach with a very dilute volume fraction. Dashed−dotted line: results based on a constant potential boundary condition. (B) Scaled surface potential as a function of $\kappa a$ at different $B$ with $A$ = 1000 and $h^*$ = 80. Dashed lines: results based on a cell model approach with a very dilute volume fraction. Dashed−dotted line: results based on a constant potential boundary condition.

the experimental results further demonstrates the reliability of this study.

As can be observed in Figure 2, the result of setting $A$ = 10000 approaches close to the corresponding results of the constant surface potential case ($|\phi_e^*|$ = 1.1), which infers that setting $A$ = 10000 (denotes as $A \rightarrow \infty$ in Figure 2) is a sufficiently large value to stand for the constant surface potential boundary condition. For the effect of the double-layer thickness, again a small $\kappa a$ implies a thick double layer, and the absolute surface potential of the particle $|\phi_e^*|$ is high. The higher the absolute surface potential, the larger the electric driving force exerted on the particle surface, and this results in higher mobility. Clearly, $|\phi_e^*|$ decreases with the increase in $\kappa a$ at various $A$. This can be explained by resorting to the boundary condition, eq 29, which can be rewritten as

$$|\phi_e^*| = \frac{1+B}{B}\left(1 - \frac{x}{c^*}\frac{1+B}{A}\frac{\partial \phi_e^*}{\partial \eta}\right) \qquad (52)$$

If the value of $\kappa a$ becomes higher, the double layer surrounding the particle is thinner, and the potential gradient $(\partial \phi_e^*/\partial \eta)$ is


dx.doi.org/10.1021/jp2000915 |J. Phys. Chem. B 2011, 115, 6484–6494

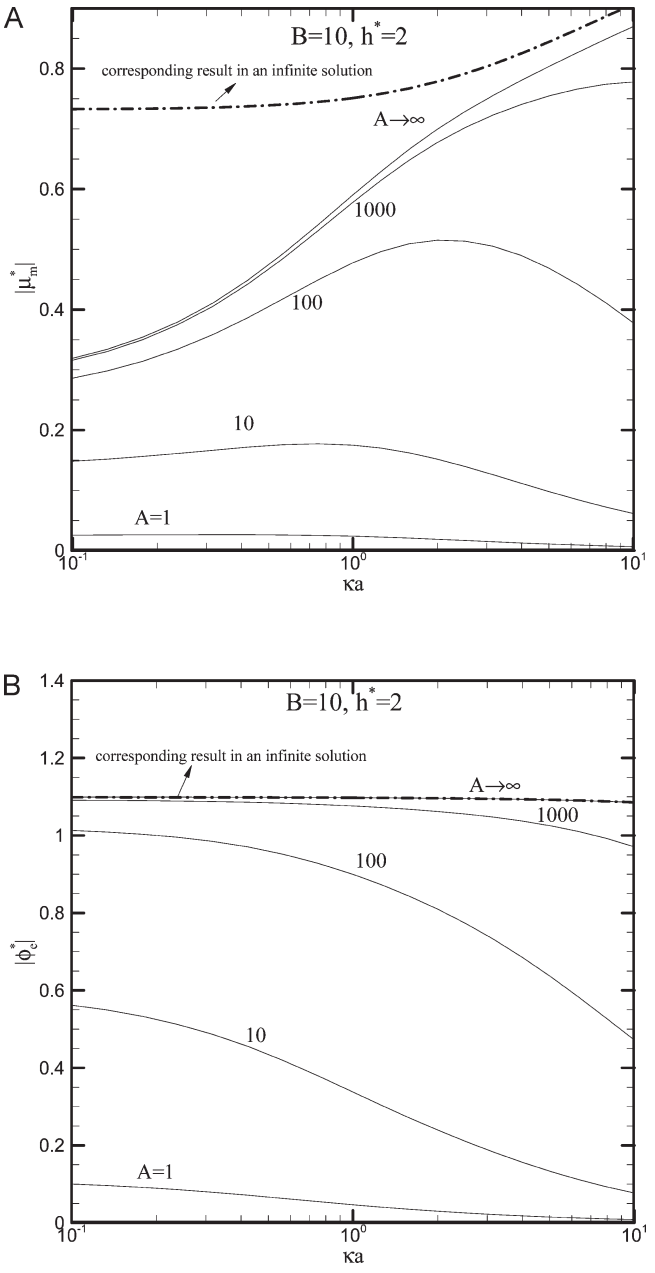


**Figure 4.** (A) Scaled mobility as a function of $\kappa a$ at different $A$ with $h^* = 2$ and $B = 10$. Dashed line: corresponding results for a single particle in an infinite medium of electrolyte solution. (B) Scaled surface potential as a function of $\kappa a$ at different $A$ with $h^* = 2$ and $B = 10$. Dashed line: corresponding results for a single particle in an infinite medium of electrolyte solution.

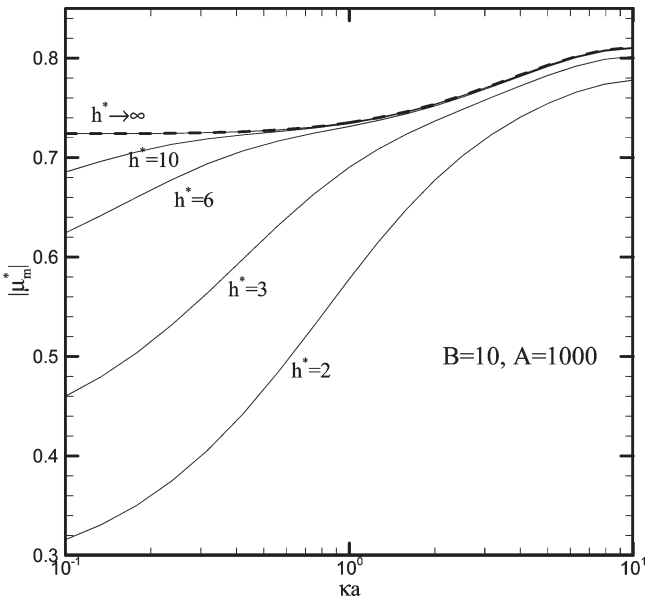


**Figure 5.** Scaled mobility as a function of $\kappa a$ at different $h^*$ with $A = 1000$ and $B = 10$. Dashed line: corresponding results for a single particle in an infinite medium of electrolyte solution based on a cell model.

larger. Because the particle is negatively charged, that is, $\partial\phi_e^*/\partial\eta > 0$, eq 52 subsequently implies that $|\phi_e^*|$ is small. Moreover, Figure 2A suggests that for fixed $\kappa a$, $|\mu_m^*|$ increases with $A$. According to its definition, a large $A$ implies that the concentration of the functional groups on the particle surface $N_s$ is high, which gives a higher surface charge density and higher $|\phi_e^*|$, as is justified by Figure 2B, therefore yielding higher mobility.

The scaled mobility $|\mu_m^*|$ and corresponding scaled surface potential $|\phi_e^*|$ as a function of $\kappa a$ at various $B$ for $h^* = 80$ is illustrated in Figure 3A and B, respectively. Figure 3B reveals that for a fixed $\kappa a$, $|\phi_e^*|$ decreases with the increase of $B$, which leads to lower mobility, as shown in Figure 3A. According to the definition of $B$, $B$ denotes the ratio of bulk concentration of $[H^+]$ to the dissociation constant $K_a$. If $K_a$ is constant, a small $B$ means that $[H^+]_0$ is small, and the bulk condition is advantageous to the dissociation reaction represented by eq 29. This has the effect of increasing $[A^-]$, and the surface charge density is increased. Note that the present model may become inapplicable if $B$ is too small. This is because the surface potential may become too high to employ the Debye–Hückel equation.

Due to the presence of a nearby air–water interface, the homogeneous double-layer shape is further deformed. As a result, all of these factors have to be considered simultaneously in order to predict the eventual particle motion. With this perception in mind, we continue to examine the particular effect of each parameter of interest. Corresponding results are presented in Figures 4–7.

**3.1. Effect of Functional Groups on the Particle Surface with the Presence of an Air–Water Interface.** Figure 4A depicts the scaled mobility $|\mu_m^*|$ as a function of $\kappa a$ at various values of $A$ at $h^* = 2$, and the corresponding results of the scaled surface potential $|\phi_e^*|$ are illustrated in Figure 4B. As discussed above, $|\phi_e^*|$ decreases with the increase in $\kappa a$, which leads to lower $|\mu_m^*|$. A large dissociated charge density on the particle surface (large $A$), which generates a higher electric driving force, tends to enhance the particle mobility as expected.

The above observations of $\kappa a$ and values of $A$ effects are consistent with the corresponding case of an isolated sphere.[21] The boundary effect of an air–water interface is analyzed in direct comparison with results of the isolated particle. Compared with Figures 4B and 2B for the electric surface potential of the particle, we find that the magnitude of the absolute surface potential of the particle is not influenced by the presence of an air–water interface, which is considered solely a function of the dissociated surface functional groups ($A = ae^2N_s/\varepsilon k_BT$), the bulk condition ($[H^+]_0/K_a$), and the double-layer thickness ($\kappa a$). The presence of the air–water interface, however, significantly deters the particle motion, especially when the double layer is thick. On the other hand, this boundary effect is observed to diminish as the

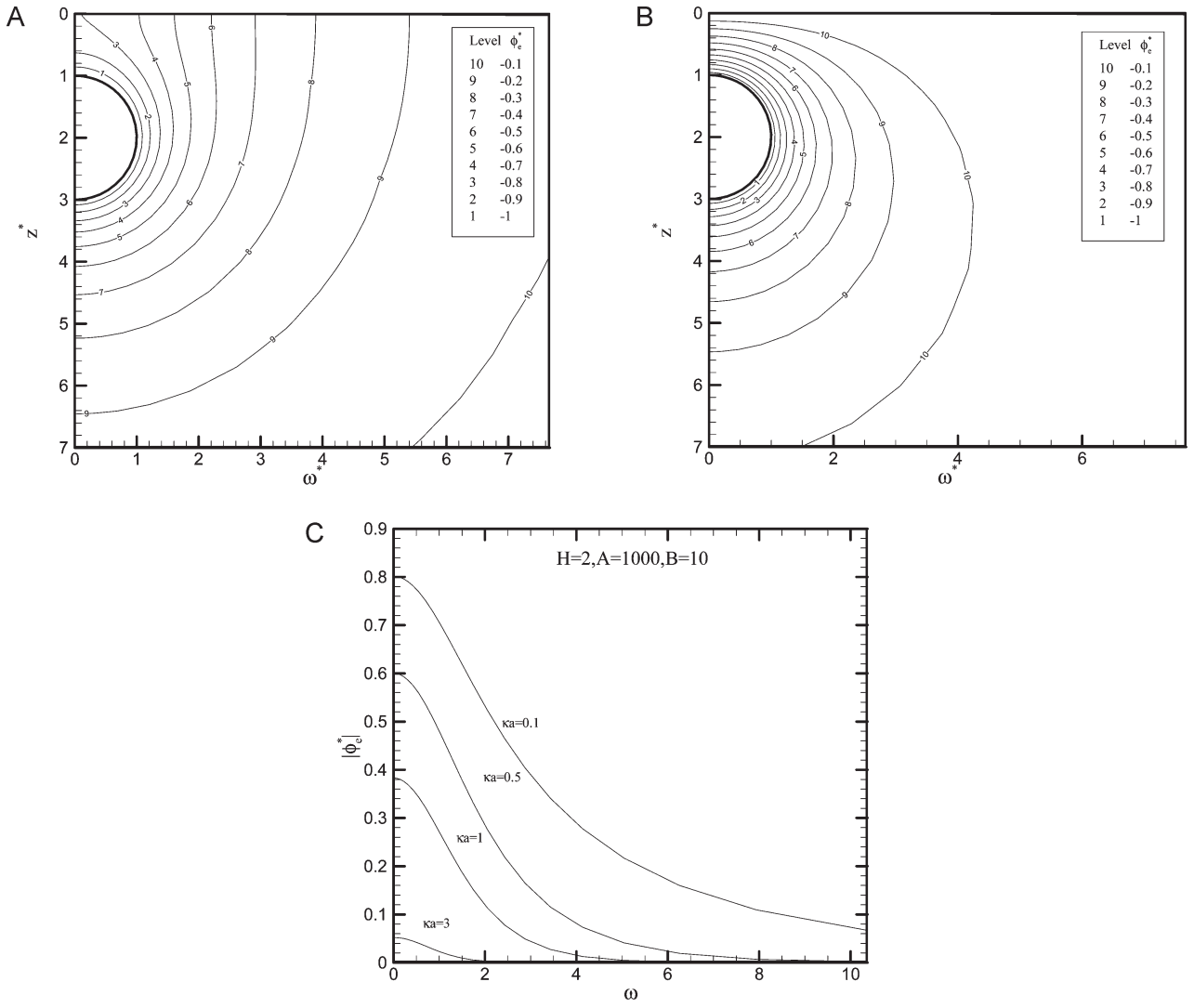


**Figure 6.** (A) Contours of a scaled equilibrium electric potential ($\phi_e^*$) with $\kappa a = 0.1$, $h^* = 2$, $A = 1000$, and $B = 10$. The top edge corresponds to the location of an air−water interface. (B) Contours of a scaled equilibrium electric potential ($\phi_e^*$) with $\kappa a = 0.1$, $h^* = 2$, $A = 1000$, and $B = 10$. The top edge corresponds to the location of a solid planar wall. (C) Distribution of the scaled equilibrium electric potential ($\phi_e^*$) along the air−water interface at different $\kappa a$ with $h^* = 2$, $A = 1000$, and $B = 10$.

double layer is very thin. Here, "thin" refers to the fact that the double layer does not touch the interface. The compression and even collapse of the double layer due to the presence of the air−water interface drastically affect the electrical potential gradient between the particle and the interface as well as the particle electrophoretic mobility, consistent with our previous study (constant surface potential case).[10] The reduction of the particle mobility due to the presence of the air−water interface serves as a proper measurement of the boundary effect. Up to 60% reduction of the particle mobility is observed at $h^* = 2$ for $A = 10000$ when the double layer is very thick ($\kappa a \cong 0.1$). This observation is consistent with the fact that the thicker the double layer, the more likely it may be deformed to a significant extent by the interface.

In general, the thicker the double layer, the more significant the boundary effect. It tends to slow down the particle motion as the double layer begins to touch or has touched the interface. Moreover, the boundary effect depends on the exact location of the particle away from the air−water interface. The effect of the separation distance between the particle and the air−water interface will be further examined in the following section.

**3.2. Influence of the Distance to the Air−Water Interface.** Figure 5 shows the scaled mobility as a function of $\kappa a$ at various $h^*$ for $A = 1000$ and $B = 10$. It is found that the larger the distance away from the interface, the larger the mobility as the boundary effect diminishes with the increasing distance in general.

As can be measured in Figure 5, the boundary effect due to the presence of a nearby air−water interface amounts to a reduction of mobility roughly by around 60% for a thicker double layer ($\kappa a = 0.1$) to around 7% for relatively thin double layer ($\kappa a = 3$) at $h^* = 2$. In general, the boundary effect gets more significant when the particle gets closer to the interface or the double layer surrounding the particle gets thicker. Figure 5 provides useful information to estimate the boundary effect of a real system.

There are some experimental reports manipulating a single colloidal particle near or at the air−water interface in the field of electrostatics as well, such as the one by Ducker et al.,[45] who measured the DLVO forces in the bubble−silica particle interactions in

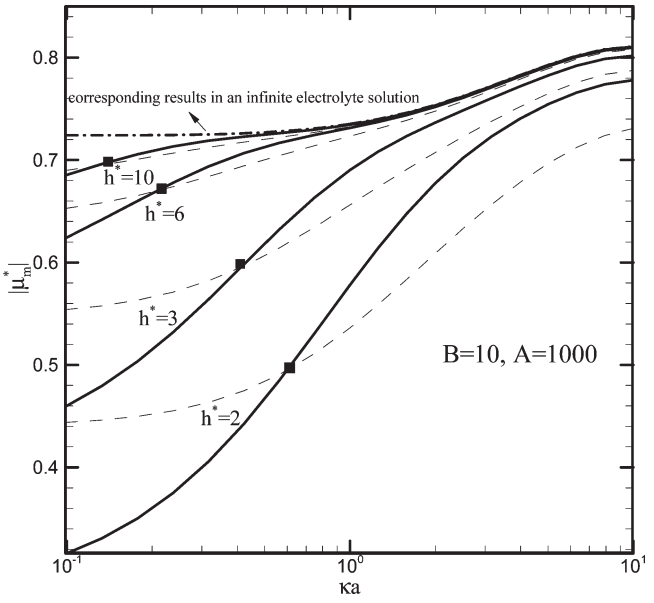


**Figure 7.** Scaled mobility as a function of $\kappa a$ at different $h^*$ with $A$ = 1000 and $B$ = 10. Dashed lines: results of a solid planar wall.

aqueous solutions by using the atomic force microscope (AFM). They found that some energy barrier of electrostatic origin exists for the particle approaching the air−water interface. Moreover, the concentration of electrolyte solution is found to play an important role in the adsorption of particles at an air−water interface there. MacRitchie and Alexander,[46] on the other hand, studied experimentally the adsorption rate of the charged globular proteins to the air−water interface. By adding NaCl salts, the rate of adsorption was found to increase when the salt concentration was increased. The above experimental findings had been explained by the theoretical study of Mbamala and Grunberg[2] via detailed calculations based on the nonlinear Poisson−Boltzmann theory regarding ion distribution. According to their study, the air−water interface forms an electrostatic energy barrier near it, which in turn generates an electrostatic repulsion force on the particle (image-charge analogue). This repulsion may prevent the colloid from adsorbing to the interface. Moreover, they found that when the salt concentration is increased, the strength of the electrostatic adsorption barrier is lowered accordingly. The particles might then overcome this barrier and eventually "pop out" and be trapped at the air−water interface, forming the two-dimensional colloidal crystal. The above experimental and theoretical findings are consistent with our results here that the boundary effect, or the particle−interface interaction, is decreased with increased $\kappa a$. That is, the boundary effect in terms of the reduction of particle mobility is much more significant when the double layer is thick and diminishes when it gets very thin, as shown in Figure 5, where the reciprocal of $\kappa a$ represents the double-layer thickness. Note that $\kappa$ is proportional to the square root of the ionic strength of the suspending electrolyte (salt) solution. The ionic strength is defined as $(1/2)\Sigma c_j z_j^2$, where $c_j$ is the ionic concentration in mol/L$^{-1}$ and $z_j$ is the valence of ionic species $j$.[31] The higher the salt solution, the larger the value of $\kappa$ and, hence, $\kappa a$, or a thinner double layer.

**3.3. Characteristics of an Air−Water Interface in Terms of the Electric Potential Distribution: Comparison with a Solid Planar Wall.** The contour plots of the equilibrium electric potential around the particle as well as its distribution profile at the interface are illustrated in Figure 6A for $A$ = 1000, $B$ = 10, $\kappa a$ = 0.1, and $h^*$ = 2. The contours can represent the actual shape of the double layer in the physical sense. Note that at such a distance, the double layer has touched the interface.

In the corresponding case of a solid boundary with the constant electric potential surface, such as a grounded metal plane, the double layer in front of the particle is squeezed as the particle moves toward the plane. This in turn squeezes the contour plots of electric potential in front of the particle, as shown in Figure 6B. This steeper gradient of electric potential generates extra attractive force for the approaching in particle. In the case of an air−water interface, on the other hand, the electric potential contour there assumes a bell shape due to the buildup of electric potential right in front and the associated outward horizontal fluid flow, as shown in Figure 6C. This potential buildup of the same sign in front of the particle generates a repulsive electrostatic force and hence slows down its motion. Further detailed analyses were given by Tsai et al.[10] as well regarding this issue, where the electrophoresis of a particle with constant surface potential was analyzed near an air−water interface.

The $\kappa a$ dependence of the electric potential profile at the free surface is further illustrated in Figure 6C. In general, a thinner double layer yields a smaller amount of the electric potential buildup at the air−water interface, which in turn yields a flatter electric potential profile. This is because the counterions are sparse outside of the double layer. When the double layer is thinner, fewer counterions exist near the interface to enable a buildup of electric potential above the reference value corresponding to a neutral bulk solution. Therefore, as the double layer gets very thin, the electric potential profile will be very close to that of a solid planar wall.

Figure 7 illustrates the scaled mobilities as a function of $\kappa a$. Note that dashed lines correspond to a solid planar wall, whereas the solid ones correspond to an air−water interface. Figure 7 reveals that for a fixed $\kappa a$, the mobility increases with its distance from either boundary in general, as expected. As $\kappa a$ is low, the particle mobility toward an air−water interface is smaller than that toward a solid planar wall. In addition, the smaller the $\kappa a$, the larger the discrepancy between these two boundary effects. The reason for it was discussed earlier for the corresponding case of a particle with a constant surface potential,[10] which is valid here as well. In short, the air−water interface retards the particle motion more severely than a solid wall when the double layer is thick enough to touch the interface and yields an electrostatic potential buildup there, as explained earlier in this section. On the other hand, when the double layer does not touch the interface, the hydrodynamic drag force, which slows down the particle motion, in general becomes the determining factor instead. The air−water interface in this case retards the particle motion less severely than a solid planar wall does as the fluid is allowed to move in the tangential direction. Therefore, the mobility normal to the interface will be larger now instead. Between these two limiting cases there exists a threshold value of $\kappa a$ where both boundaries yield the same mobility, as shown in Figure 7 by the symbol ■. Note that the locations of these threshold values of $\kappa a$ correspond roughly to the situation when the double layers touch the boundaries.

## 4. CONCLUDING REMARKS

Electrophoresis of a charge-regulated sphere normal to an air−water interface is investigated theoretically. A general mixed-type

condition results on the particle surface when the surface potential is low. The conventional models, which assume either constant surface potential or constant surface charge, can be recovered easily as the special cases of the present analysis. In particular, the behavior of biological cells, which carry dissociable functional groups, and particles which are capable of exchanging ions with the surrounding medium can be simulated by the present model. Key parameters of electrokinetic interest are examined to explore their respective effect on the particle electrophoretic mobility. Moreover, a detailed comparison with the corresponding solid planar wall is carried out to examine unique boundary effects and phenomena associated with the air−water interface in particular.

Numerical results reported in the literature for an isolated particle associated with a charge-regulated surface valid at low potential are recovered excellently when the particle is far away from the interface. It is found that the electric potential on particle surface is one of the dominant factors in the determination of the eventual particle electrophoretic mobility. In general, the larger the number of dissociated functional groups on particle surface ($N_s$), the higher the particle surface potential and hence the larger the magnitude of the particle mobility. Moreover, the electric potential on the particle surface depends on both the concentration of dissociated hydrogen ions $[H^+]_0$ and the concentration of electrolytes $\kappa a$ in the solution. If $[H^+]_0$ and/or $\kappa a$ is small, the bulk condition is advantageous to the dissociation reaction, yielding a higher surface density (higher surface potential) and hence a higher mobility.

The presence of the air−water interface is found to reduce the particle mobility, especially when the double layer is very thick. Up to around 60% mobility, reduction is observed, for instance, for $h^* = 2$ when the double layer is very thick. This boundary effect diminishes as the double layer becomes very thin, on the other hand. This is a direct consequence of the deformation or even the collapse of the double layer by the presence of the air−water interface. This results in the redistribution of ions in the double layer, which affects the eventual electrophoretic motion of the particle.

Finally, comparison with a corresponding solid planar boundary is carried out to highlight the fundamental nature of an air−water interface. The air−water interface tends to retard the particle motion more severely when the double layer touches the interface, and otherwise when it does not. The reason behind it is mainly due to the buildup of electric potential at the air−water interface, which reduces the electric driving force of the particle in a way resulting in the above observations.

## AUTHOR INFORMATION

### Corresponding Author

*Tel: +886-2-23622530. Fax: +886-2-23622530. E-mail: ericlee@ntu.edu.tw.

## ACKNOWLEDGMENT

This work is finically supported by the National Science Council of the Republic of China.

## REFERENCES

(1) Terao, T.; Nakayama, T. *Phys. Rev. E* **1999**, *60* (6), 7157–7162.
(2) Mbamala, E. C.; von Grunberg, H. H. *J. Phys.: Condes. Matter.* **2002**, *14* (19), 4881–4900.
(3) Sanchez, C. C.; Nino, M. R. R.; Caro, A. L.; Patino, J. M. R. *J. Food Eng.* **2005**, *67* (1−2), 225–234.
(4) Hayes, C. F. *J. Phys. Chem.* **1975**, *79* (16), 1689–1693.
(5) Arisawa, S.; Yamamoto, R. *Langmuir* **1993**, *9* (4), 1028–1030.
(6) Sugiyama, Y.; Inoue, T.; Ikematsu, M.; Iseki, M.; Sekiguchi, T. *Jpn. J. Appl. Phys., Part 1* **1997**, *36* (9A), 5674–5679.
(7) Huddleston, R.; Smith, A. *Foams*; Academic Press: New York, 1976.
(8) Usui, S.; Healy, T. W. *J. Colloid Interface Sci.* **2001**, *240* (1), 127–132.
(9) Gao, Y. D.; Li, D. Q. *J. Colloid Interface Sci.* **2008**, *319* (1), 344–352.
(10) Tsai, P.; Lou, J.; He, Y. Y.; Lee, E. *Electrophoresis* **2010**, *31* (20), 3363–3371.
(11) Krozel, J. W.; Saville, D. A. *J. Colloid Interface Sci.* **1992**, *150* (2), 365–373.
(12) Ninham, B. W.; Parsegia, Va. *J. Theor. Biol.* **1971**, *31* (3), 405–.
(13) Carnie, S. L.; Chan, D. Y. C. *J. Colloid Interface Sci.* **1993**, *155* (2), 297–312.
(14) Carnie, S. L.; Chan, D. Y. C. *J. Colloid Interface Sci.* **1993**, *161* (1), 260–264.
(15) Carnie, S. L.; Chan, D. Y. C.; Gunning, J. S. *Langmuir* **1994**, *10* (9), 2993–3009.
(16) Carnie, S. L.; Chan, D. Y. C.; Stankovich, J. *J. Colloid Interface Sci.* **1994**, *165* (1), 116–128.
(17) Menon, M. K.; Zydney, A. L. *Anal. Chem.* **2000**, *72* (22), 5714–5717.
(18) Kuo, Y.; Hsieh, M.; Hsu, J. *J. Phys. Chem. B* **2002**, *106* (16), 4255–4260.
(19) Hong, Y.; Brown, D. *Colloids Surf. B: Biointerfaces* **2006**, *50* (2), 112–119.
(20) Hong, Y.; Brown, D. *Langmuir* **2008**, *24* (9), 5003–5009.
(21) Lee, E.; Yen, F. Y.; Hsu, J. P. *Electrophoresis* **2000**, *21* (3), 475–480.
(22) Hsu, J. P.; Lee, E.; Yen, F. Y. *J. Chem. Phys.* **2000**, *112* (14), 6404–6410.
(23) Tang, Y. P.; Chih, M. H.; Lee, E.; Hsu, J. P. *J. Colloid Interface Sci.* **2001**, *242* (1), 121–126.
(24) Hsu, J.; Ku, M.; Kuo, C. *Langmuir* **2005**, *21* (16), 7588–7597.
(25) Hsu, J.; Kuo, C.; Ku, M. *Electrophoresis* **2008**, *29* (2), 348–357.
(26) Hsu, J.; Chen, C.; Lee, D.; Tseng, S.; Su, A. *J. Colloid Interface Sci.* **2008**, *325* (2), 516–525.
(27) Israelachvili, J. N. *Intermolecular and surface forces*; Academic Press: New York, 1985; Chapter 11.
(28) Lou, J.; Shih, C. Y.; Lee, E. *J. Colloid Interface Sci.* **2009**, *331* (1), 227–235.
(29) Huang, C. H.; Cheng, W. L.; He, Y. Y.; Lee, E. *J. Phys. Chem. B* **2010**, *114* (31), 10114–10125.
(30) Brenner, H. *Chem. Eng. Sci.* **1961**, *16* (3−4), 242–251.
(31) Hunter, R. J. *Foundations of colloid science*; Clarendon Press: Oxford, U.K., 1989.
(32) Onsager, L.; Samaras, N. *J. Chem. Phys.* **1934**, *2*, 528.
(33) Levin, Y. *J. Chem. Phys.* **2000**, *113*, 9722–9726.
(34) Ohshima, H.; Matsubara, H. *Colloid Polym. Sci.* **2004**, *282* (9), 1044–1048.
(35) Markovich, G.; Giniger, R.; Levin, M.; Cheshnovsky, O. *J. Chem. Phys.* **1991**, *95*, 9416–9419.
(36) Ghosal, S.; Hemminger, J. C.; Bluhm, H.; Mun, B. S.; Hebenstreit, E. L. D.; Ketteler, G.; Ogletree, D. F.; Requejo, F. G.; Salmeron, M. *Science* **2005**, *307*, 563–566.
(37) Garrett, B. C. *Science* **2004**, *303*, 1146–1147.
(38) Pavel, J.; Douglas, J. T. *Chem. Rev.* **2006**, *106* (4), 1259–1281.
(39) Horinek, D.; Netz, R. R. *Phys. Rev. Lett.* **2007**, *99*, 226104.
(40) Levin, Y.; dos Santos, A. P.; Diehl, A. *Phys. Rev. Lett.* **2009**, *103* (25), 257802.
(41) Henry, D. *Proc. R. Soc. London, Ser. A* **1931**, 106–129.
(42) Ohshima, H. *Theory of colloid and interfacial electric phenomena*; Academic Press: New York, 2006.

(43) O'Brien, R.; White, L. *J. Chem. Soc., Faraday Trans. 2* **1978**, *74*, 1607–1626.
(44) Heard, D. H.; Seaman, G. V. F. *J. Gen. Physiol.* **1960**, *43* (3), 635–654.
(45) Ducker, W. A.; Xu, Z. G.; Israelachvili, J. N. *Langmuir* **1994**, *10* (9), 3279–3289.
(46) Macritchie, F.; Alexander, A. E. *J. Colloid Interface Sci.* **1963**, *18* (5), 464.